INORGANIC CHEMISTRY FRONTIERS

CCS 中国化学会 CHINESE CHEMICAL SOCIETY

ROYAL SOCIETY OF CHEMISTRY

Stabilized photoemission from organic molecules in zero-dimensional hybrid Zn and Cd halides

Journal:	*Inorganic Chemistry Frontiers*
Manuscript ID	QI-RES-06-2022-001293.R1
Article Type:	Research Article
Date Submitted by the Author:	30-Sep-2022
Complete List of Authors:	Creason, Tielyr; University of Oklahoma, Department of Chemistry & Biochemistry Fattal, Hadiah; University of Oklahoma, Department of Chemistry & Biochemistry Gilley, Isaiah; University of Oklahoma, Department of Chemistry & Biochemistry Evans, Brett; University of Oklahoma, Department of Chemistry & Biochemistry Jiang, Jie; Air Force Research Laboratory, Materials & Manufacturing Directorate Pachter, Ruth; Air Force Research Laboratory, Materials & Manufacturing Directorate Glatzhofer, Daniel T.; University of Oklahoma, Department of Chemistry & Biochemistry Saparov, Bayram; University of Oklahoma, Department of Chemistry & Biochemistry

Stabilized photoemission from organic molecules in zero-dimensional hybrid Zn and Cd halides

*Tielyr D. Creason,[1] Hadiah Fattal,[1] Isaiah W. Gilley,[1] Brett N. Evans,[1] Jie Jiang,[2] Ruth Pachter,[2] Daniel T. Glatzhofer,[1] and Bayram Saparov[1]**

[1]Department of Chemistry and Biochemistry, University of Oklahoma, 101 Stephenson Parkway, Norman, OK, USA
[2]Air Force Research Laboratory, Materials and Manufacturing Directorate, Wright-Patterson Air Force Base, OH, USA

*Corresponding authors: saparov@ou.edu

Abstract

This work explores the utilization of a photoactive organic cation for the preparation of R_2MCl_4 (M = Zn, Cd; R = (*E*)-4-styrylpyridinium, $C_{13}H_{12}N^+$). The zero-dimensional crystal structures of R_2MCl_4 contain isolated tetrahedral anions $[MCl_4]^{2-}$ separated by the organic cations R^+, leading to flat bands around the optical band gap. In R_2MCl_4, the inorganic band gaps are sufficiently large to accommodate the organic molecular levels within, and therefore, the optical properties of R_2MCl_4 are determined by the organic cation. Our combined optical spectroscopy and density functional theory (DFT) studies confirm the attribution of the bright green photoluminescence demonstrated by R_2MCl_4 to the organic molecular emission. Importantly, the incorporation of the photoemissive organic cation R^+ into the hybrid framework in R_2MCl_4 leads to a nearly two-fold enhancement of the light emission efficiency with the measured photoluminescence quantum yield (PLQY) values of 6.04%, 10.40% and 11.21% for RCl, R_2ZnCl_4 and R_2CdCl_4, respectively. In addition, the crystal structure of the hybrid R_2MCl_4 ensures a stabilized PL emission, preventing the occurrence of the harmful organic photodimerization, which is a notorious problem for this class of organic emitters.

Introduction

In recent years, low-dimensional hybrid organic-inorganic metal halides have emerged as materials of interest due to their outstanding optical properties, including tunability of their photoluminescence emission (PL) and high photoluminescence quantum yield (PLQY) values.[1-14] In fact, low-dimensional hybrid organic-inorganic metal halides constitute an extensive family encompassing 2D layered, 1D chain, and 0D cluster structures containing a virtually limitless selection of organic cations of various sizes, shapes, and electronic properties and *p*- and *d*-block metals.[15-17] Such a rich compositional and structural playground allows materials chemists to test a variety of materials design, synthesis, and physical property-oriented ideas.

Historically, the inorganic structural component has been the primary focus of research when targeting high-efficiency hybrid metal halide light emitters.[18-23] A fundamental shift in materials design strategy is the use of a photoactive organic molecule as the source of light emission.[24, 25] Unlike the case of the metal halide derived photoemission, in which small variations in the coordination environments of metals can cause significant and unpredictable changes in PL, in principle, an organic molecule derived emission is comprised of well-defined HOMO-LUMO transitions from isolated moieties. Although the predictability of transitions has tradeoffs, organic-derived PL emission can often be unstable, e.g., over time, organic-derived emission often quenches due to low photostability.[26-28] Through targeted synthesis, the inclusion of organic light emitters into a hybrid organic-inorganic compound can increase light emission efficiency and improve stability. However, selecting specific metals and halogens is vital to ensure emission originates from the organic component, i.e., the choice of an electronegative metal (e.g., Pb or Bi) and heavy halogen such as I often prevents the organic emission due to the inorganic band-to-band transitions. On the other hand, the more electropositive group 12 metals such as Zn and Cd paired with the more electronegative Cl present a unique solution to this problem, as their expected band gaps are high enough to allow for the organic molecular emission.[24, 29, 30]

This work reports the crystal structures and optical properties of two compounds, R_2MCl_4 (M = Zn, Cd; R = (*E*)-4-styrylpyridinium, $C_{13}H_{12}N^+$), which were prepared following the above-described materials design strategy. Styrylpyridine and styrylpyridine-derived compounds have been studied previously as organic phosphors, and the compound excels particularly due to its competitive PLQY and the PL tunability afforded by the aromatic ring substitutions.[31-33] While the organic salt has desirable optical characteristics, in-depth studies are limited due to its poor stability and tendency to photodimerize.[34] The crystal structure of R_2ZnCl_4 has been previously reported, whereas R_2CdCl_4 is a novel compound reported here for the first time.[35] R_2MCl_4 were studied using X-ray diffraction, optical spectroscopy, thermogravimetry (TGA) and differential scanning calorimetry (DSC) measurements, and density functional theory (DFT) calculations. A nearly two-fold increase in light emission efficiencies was measured for R_2MCl_4 as compared to the precursor organic salt RCl. In addition, a marked improvement in light emission stability is reported, eliminating the parasitic photodimerization issue.

Experimental

Chemicals. Zinc chloride (98%+, Fischer Scientific), Cadmium chloride (99%+, Thermo Scientific), and 4- picoline (99%, Thermo Scientific) were purchased and used as received.

Synthesis of RCl (Scheme 1). (*E*)-4-Styrylpyridine was synthesized by condensation of 4-picoline with benzaldehyde in acetic anhydride using literature procedures.[36, 37] (*E*)-4-Styrylpyridinium chloride (RCl) was obtained by dissolving (*E*)-4-styrylpyridine in a sufficient amount of aqueous hydrochloric acid, then allowing evaporation to occur until long needles formed, which were collected by filtration and allowed to dry (Fig. S1)[38, 39]

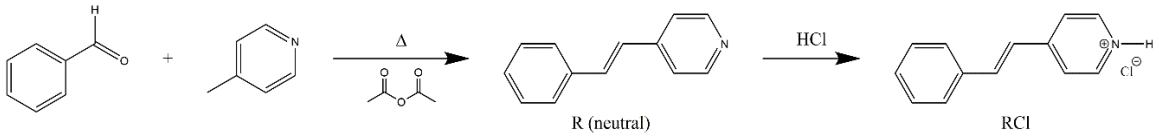

Scheme 1. Synthesis of the organic salt RCl.

Synthesis of $RMCl_4$ (M = Zn, Cd). In a typical procedure, 0.250 mmol M(II) chloride (Aldrich or Fisher) was dissolved in 2.0 mL distilled water. (*E*)-4-Styrylpyridine (0.500 mmol) was suspended in 2.0 mL distilled water and concentrated hydrochloric acid was added dropwise (2-5 drops) with agitation until all the (*E*)-4-styrylpyridine had dissolved. The (*E*)-4-styrylpyridinium chloride solution was combined with the MCl_2 solution and the container was rinsed with a small amount of distilled water that was then added to the mixture. For M = Zn, the resulting clear solution was allowed to evaporate at room temperature to form needle crystals (Fig. S2) which were isolated by filtration and allowed to dry. For M = Cd, a precipitate formed, and distilled water was added dropwise with warming until the solution was clear. This solution was allowed to cool to room temperature and evaporate, forming needle crystals (Fig. S2) which were isolated by filtration and allowed to dry. Formation of R_2MCl_4 using the above procedures was very flexible and scaled up as needed. Formation of R_2MCl_4 crystals could also be achieved by dissolving the organic precursor salt (*E*)-4-styrylpyridinium chloride (RCl) in water and combining with an appropriate amount of aqueous M(II) chloride solution, followed by evaporation at room temperature. Crystals of R_2MCl_4 formed by either method were checked for purity using PXRD before further use.

Single Crystal X-Ray Diffraction (SXRD) Measurements. Single crystal X-ray diffraction (SXRD) data were collected at 100(2) K on a Bruker D8 Quest with a Kappa geometry goniometer, an Incoatec Imus X-ray source (graphite monochromated Mo-Kα (λ = 0.71073 Å) radiation), and a Photon II detector. The data were corrected for absorption using the semiempirical method based on equivalent reflections, and the structures were solved by intrinsic phasing methods (SHELXT) as embedded in the APEX3 v2015.5-2 program. All atoms were refined with anisotropic displacement parameters and site occupancy factors were checked by freeing occupancies of each unique crystallographic site. Details of the data collection, crystallographic parameters and atomic coordinates are summarized in Tables S1-S3. Additional information on the crystals structure investigations can be obtained in the form of a Crystallographic Information File (CIF), which was

deposited in the Cambridge Crystallographic Data Centre (CCDC) database (deposition number 2178148).

Powder X-ray Diffraction (PXRD) Measurements. In order to establish bulk purity, PXRD measurements were performed on a Rigaku Miniflex600 benchtop diffractometer with a D/tex detector and a Ni-filtered Cu-Kα radiation source. The scans were done with room temperature measurements in the 3-90° (2θ) range using a step size of 0.02°. The PXRD data were fitted using the Pawley method (Fig. S3). Room-temperature PXRD measurements were also taken on a single crystal using the above-described conditions. In order to test for air and moisture stability of the compounds, periodic PXRD measurements were taken on samples stored in open air (thermostat set to 20 °C and 30% relative humidity).

Thermal Property Measurements. Simultaneous thermogravimetric analysis (TGA) and differential scanning calorimetry (DSC) measurements were performed on a polycrystalline powdered sample of R_2MCl_4 and RCl on a TA Instruments SDT 650 thermal analyzer system. Samples were heated up from 25 to 300 °C under an inert flow of dry nitrogen gas at a rate of 100 mL/min, with a heating rate of 5 °C/min.

Melting point measurements for R_2MCl_4 and RCl were run on a Mel – Temp apparatus, 110/120VAC, 50/60 Hz, 200W. The heating element was set to 50 volts, and the measurements took 15 minutes and 20 minutes for R_2MCl_4 and RCl, respectively. The samples were loaded in the capillary tubes (0.8 – 1.1 × 90 mm).

Optical Property Measurements. Photoluminescence emission (PL) and excitation (PLE) measurements were performed at room temperature using a Jobin Yvon Fluorolog-3 spectrofluorometer (HORIBA company) equipped with a Xenon lamp and a Quanta-φ integrating sphere. PL and PLE experiments were conducted on single crystals and polycrystalline powder samples of R_2ZnCl_4 and R_2CdCl_4. The same measurements were also completed for both single crystals and polycrystalline powder samples of the precursor organic salt RCl. For lifetime measurements, a Time-Correlated Single Photon Counting (TCSPC) system including a DeltaHub DH-HT high throughput TCSPC controller and NanoLED NL-C2 pulsed diode controller was used. For light source, a 350 nm NanoLED diode was selected, which has a <1.2 ns pulse duration.

For the photostability measurements, single crystals of R_2ZnCl_4 and R_2CdCl_4 and powder samples of RCl were placed inside the Quanta-φ integrating sphere on the Jobin Yvon Fluorolog-3 spectrofluorometer. The samples were then exposed to the full power of the Xenon lamp of the spectrofluorometer at the PL excitation maximum of 445 nm and 453 nm for R_2ZnCl_4 and R_2CdCl_4, respectively. Periodic PLQY measurements were taken every 5 minutes under these conditions over 60 minutes.

Room temperature diffuse reflectance spectra of polycrystalline powder of $RZnCl_4$ and $RCdCl_4$ were measured using a high-resolution PerkinElmer LAMBDA 750 UV−vis−NIR spectrometer equipped with a 100 mm InGaAs integrating sphere attachment. The diffuse reflectance data were converted to pseudo absorption spectra according to the Kubelka-Munk equation, $FI = \alpha/S = (1-R)^2/(2R)$, where R is the reflectance, α is the absorption coefficient, S is the scattering coefficient.

Computational Details. DFT calculations were carried out with the Vienna ab initio simulation package VASP 5.4.[40, 41] The Kohn-Sham equations are solved using a plane wave basis set with an energy cutoff of 550 eV, and the projector augmented-wave (PAW) potential was applied.[41] A 2×3×2 *k*-point sampling was used for the monoclinic primitive cell for the R_2MCl_4 0D perovskites, e.g. for R_2CdCl_4, which has lattice constants of 15.037 Å, 11.808 Å, and 14.440 Å. The structures were optimized using the Perdew−Burke−Ernzerhof (PBE) functional,[42] including the zero damping D3 correction of Grimme,[43] as inclusion of London dispersion for treating halide perovskites was emphasized,[44] and previously applied.[45] Geometries were fully relaxed regarding lattice parameters and interatomic distances until forces were less than 0.01 eV/Å. Band structures were calculated at the PBE level, unless indicated otherwise.

Results and Discussion

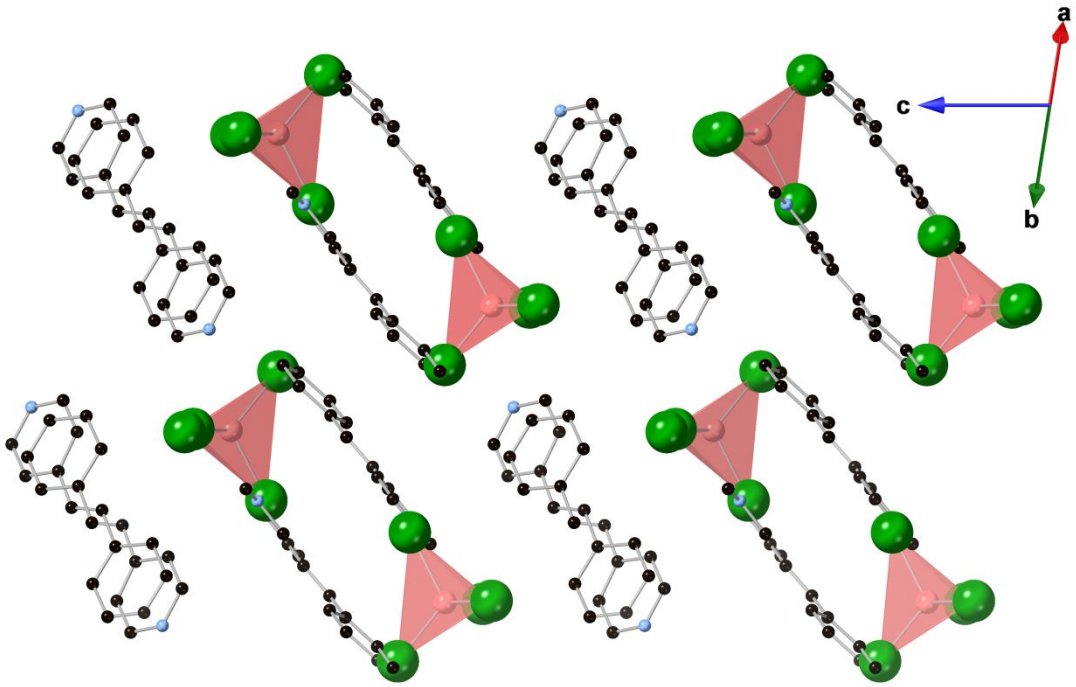

Fig. 1. The 0D crystal structure of R_2MCl_4 (M= Zn, Cd). C, N, M, and Cl atoms are shown in black, light blue, pink, and green, respectively; H atoms are omitted for clarity.

R_2ZnCl_4 and R_2CdCl_4 were both grown through the slow evaporation of water solutions of stoichiometrically loaded precursors. The facile synthesis yielded large yellow needles of up to one centimeter in length (Fig. S2). Both compounds crystalize in the monoclinic space group *C*2/*c* and contain $[MCl_4]^{2-}$ tetrahedra separated by R^+ cations in their 0D crystal structures (see Fig. 1). The organic cations form pairs wherein the phenyl group of one R^+ cation is positioned towards the pyridyl group of the other R^+ cation. In the space between organic cation pairs, there exist isolated $[MCl_4]^{2-}$ tetrahedra. The formation of this structure can be attributed to the electrostatic

interactions that occur between the pyridyl group of R^+ and $[MCl_4]^{2-}$ as well as the stacking interaction that occurs between the rings in the R^+ cations. These types of interactions are common in low-dimensional metal halide materials.[28, 31, 34]

When diving deeper into the intricacies of the structures, one finds that $[ZnCl_4]^{2-}$ tetrahedra in R_2ZnCl_4 are slightly distorted with the Zn-Cl bond distances ranging from 2.266 to 2.277 Å; the bond lengths agree well with the estimates obtained using the sum of Shannon ionic radii for Zn^{2+} and Cl^-.[46] On the other hand, a greater variation is observed for the bond angles within the $[ZnCl_4]^{2-}$ tetrahedra, which range from 104.61 to 113.71°. The presence of slightly distorted zinc chloride tetrahedra with similar bond angles and lengths has also been reported for other hybrid Zn halides in the literature. For example, in (aminoethylpiperazine)$ZnCl_4$, Zn-Cl bond lengths range from 2.258 to 2.279 Å, and bond angles range from 104.70 to 112.00° within the $[ZnCl_4]^{2-}$ tetrahedra.[47] These comparisons show that the $[ZnCl_4]^{2-}$ tetrahedra are commonly distorted in hybrid organic-inorganic zinc halides.[24, 47, 48] Since Zn^{2+} has a $3d^{10}$ electronic configuration in R_2ZnCl_4, such distortions cannot be attributed to the electronic effects such as Jahn-Teller effect (e.g. in Cu^{2+} halides) or the presence of stereochemically active lone ns^2 pair (e.g., in the case of broadband white light-emitting lead halide perovskites).[3, 14, 49, 50] Instead, the observed distortions are likely caused by crystal packing effects and the sizes, shapes and H-bonding characteristics of the organic cations that template the crystal structures.

In literature, hybrid organic-inorganic cadmium chlorides have been reported to feature both tetrahedral $[CdCl_4]^{2-}$ and octahedral $[CdCl_6]^{4-}$ building blocks.[51-54] The formability and preference for a specific coordination environment around a metal center is typically predicted following Pauling's Radius Ratio Rules using $\mu = r_M/r_X$, where r_M and r_X are the Shannon ionic radii; the acceptable range for tetrahedral structures is $\mu_{tet} = 0.225–0.414$, whereas higher $\mu_{oct} = 0.414–0.732$ range is predicted to result in octahedral structures. For Cd(II) chlorides, tetrahedral and octahedral factors of $\mu_{tet} = 0.43$ and $\mu_{oct} = 0.52$ are calculated, suggesting a preference for octahedral coordination in Cd(II) halides from purely packing efficiency arguments. Therefore, the stabilization of tetrahedral structure in R_2CdCl_4 and several other recently reported hybrid Cd(II) halides can be ascribed to the stabilization of these structures through interactions with the organic cations.[29, 30, 51, 53-56] As an indication of organic cation and inorganic anion interactions, the $[CdCl_4]^{2-}$ tetrahedra are also distorted in R_2CdCl_4, with the bond distances ranging from 2.434 to 2.464 Å, and the bond angles ranging from 100.78 to 119.26°. Depending on the organic molecular cation used to template the structure, reported hybrid cadmium halides can feature regular or distorted tetrahedral building blocks. For instance, the bond distances range from 2.4477 to 2.4626 Å in [2-methyl-3-(pyridin-2-yl)imidazo[1,5-*a*]pyridinium]$CdCl_4$. However, the bond angles of 107.08 - 108.63° show minimal deviation from the tetrahedral angle.[56] The observed variations in the bond distances and angles of hybrid Zn and Cd halides support the important role of organic cations in the structural intricacies and stability of this family of compounds.

To establish the bulk purity of the samples, powder X-ray diffraction (PXRD) measurements were collected (Fig. S3). R_2ZnCl_4 is clearly more crystalline in nature, indicated by sharp, high-intensity peaks in the PXRD. R_2CdCl_4 conversely is observably less crystalline, which is in part

attributed to the loss in crystallinity upon grinding of its single crystals. The necessary grinding causes an emergence of a small amount of the organic salt.[35] In order to test air and moisture stability of R_2ZnCl_4 and R_2CdCl_4, periodic PXRD scans over the course of several weeks were collected (Fig. S4). Both hybrid compounds are found to be air and moisture stable, with no impurities forming after several weeks of exposure to ambient air. These results indicate that R_2ZnCl_4 and R_2CdCl_4 have improved air stability when compared to the pure organic salt, which is known to be relatively unstable due to dimerization over time.[27]

Thermal properties of R_2ZnCl_4 and R_2CdCl_4 were characterized through TGA/DSC measurements (Fig. S5). For R_2ZnCl_4, an endothermic peak in DSC was measured with the onset temperature of 231.44 °C. This DSC signal is in agreement with the measured melting point of 237.5 °C for R_2ZnCl_4, which suggests that mass loss is initiated by melting. A similar TGA/DSC profile was observed for R_2CdCl_4 – here, the endothermic peak in DSC has an onset temperature of 227.96 °C, and the melting point of the compound was measured to be 231.2 °C via Mel-Temp.

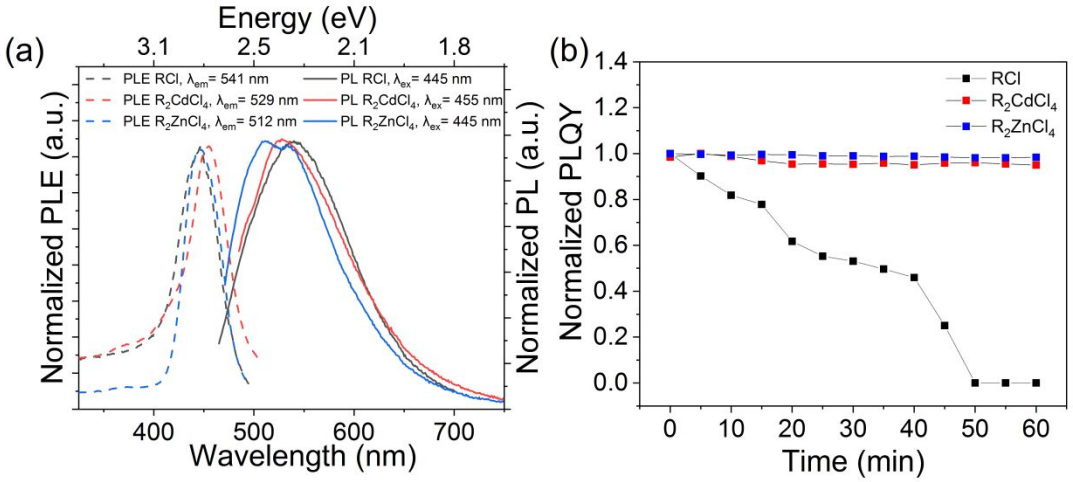

Fig. 2. (a) Normalized photoluminescence emission (PL) and excitation (PLE) spectra of RCl, R_2ZnCl_4, and R_2CdCl_4. (b) Normalized photoluminescence quantum yield (PLQY) values of RCl, R_2ZnCl_4, and R_2CdCl_4 under continuous exposure at their max excitation energy.

To evaluate their optical properties, photoluminescence emission (PL) and photoluminescence excitation (PLE) measurements were taken at room temperature for R_2ZnCl_4, R_2CdCl_4, and RCl (Fig. 2). As hypothesized, both the PL and PLE for the hybrid Zn and Cd halides have near-identical emission curves to that of the precursor organic salt RCl, indicating that the photoemission originates from the organic component in both hybrid compounds. All three compounds have similar photoluminescence emission maxima at 512 nm, 529 nm and 541 nm for R_2ZnCl_4, R_2CdCl_4 and RCl, respectively. The photoluminescence excitation maxima were measured to be at 445 nm, 453 nm and 445 nm for R_2ZnCl_4, R_2CdCl_4 and RCl, respectively. The full width at half maximum (FWHM) for R_2ZnCl_4, R_2CdCl_4 and RCl were measured to be 113 nm, 117 nm, and 117 nm, respectively. R_2ZnCl_4 demonstrates a bright green emission (Fig. S6) with the Commission Internationale de l'Eclairage (CIE) color coordinates of (0.28, 0.51). R_2CdCl_4 shows a green-yellow emission (Fig. S6) with the CIE color coordinates of (0.34, 0.55). The minor

difference in the emission colors is due to the lack of intensity in the higher energy shoulder for R_2CdCl_4. In comparison, the organic salt RCl exhibits a nearly identical yellow light emission profile relative to R_2CdCl_4 with the CIE coordinates of (0.36, 0.54). Importantly, while the emission profiles are similar in these three compounds, there is a significant enhancement of the light emission in the hybrid materials as compared to the organic salt. The measured PLQY values were 10.40% and 11.21% for R_2ZnCl_4 and R_2CdCl_4, respectively, while the PLQY for the organic salt was 6.40%. Notably, these PLQY values compare well to that of other reported hybrid organic-inorganic zinc and cadmium halides (Table 1).

Table 1. Photophysical properties of various hybrid organic-inorganic zinc/cadmium halides.[24, 29, 47]

Compound	PLQY (%)	PL_{max} (nm)	PLE_{max} (nm)	Stokes Shift (nm)	FWHM (nm)	Ref
R_2ZnCl_4	10.40	512	445	67	113	this work
R_2CdCl_4	11.21	528	453	75	117	this work
$(C_5H_7N_2)_2ZnBr_4$	19.18	438	320	118	-	[24]
$[C_6(CH_3)_5CH_2N(CH_3)_3]_2CdBr_4 \cdot DMSO$	0.32	501	399	102	164	[29]
$(C_6(CH_3)_5CH_2N(CH_3)_3)ZnBr_3(DMSO)$	3.07	491	386	105	188	[29]
(N-aminoethylpiperazine)$ZnCl_4$	11.52	400	300	100	184	[47]

In addition to an increase in the PL efficiency, an important added goal of this study is the improvement of photostability of the organic component embedded in the hybrid metal halide structure. To evaluate their photostability, the samples were continuously exposed to high-intensity UV light during the 1-hour testing period with periodic measurements of PLQY values (Fig. 2b). As expected, the PLQY of RCl fully degrades within one hour, whereas the PL emission intensity of R_2ZnCl_4 and R_2CdCl_4 remain consistent, with negligible PLQY losses. These results indicate the viability of utilization of organic emitters in hybrid metal halide structures, and that the combination of the organic emitter and inorganic metal halide into one structure substantially improve the photostability of the organic emitter.

To understand the difference in photostability a detailed structural examination was completed. It is known that the parent stilbazole hydrochloride salt in the solid-state undergoes facile [2+2] photodimerization of the central carbon-carbon double bond to form the corresponding tetrasubstituted cyclobutane compound.[57] The enhanced photostability of hybrid structures R_2ZnCl_4 and R_2CdCl_4 is likely due to a combination of two structural factors. First, in the structures of R_2ZnCl_4 and R_2CdCl_4, the co-facial distance between the central carbon-carbon double bonds of the neighboring stilbazole moieties increases from 3.797 Å for the hydrochloride salt to 4.218 Å and 4.286 Å, respectively.[27, 35] These distances are above the commonly accepted range of 3.5

– 4.2 Å for photodimerization to occur.[26] Since these distances in hybrid halides are just beyond 4.2 Å, it might be expected that dimerization and photo-deactivation could slowly occur, especially as heating occurs with irradiation. However, a second structural factor that may be hindering the photodimerization in R_2ZnCl_4 and R_2CdCl_4 and enhancing their photostability is the crystal lattice itself. Dimerization of the stilbazole moiety causes a significant structural reorganization. The distance between the central carbon-carbon double bonds contracts from 3.797 Å in RCl to ca. 1.55 Å on dimerization and formation of the cyclobutene ring, while the distance between the nitrogen and the *para*-carbon on the opposing stilbazole benzene ring expands from 3.933 Å in RCl to >5.4 Å, accompanied by considerable twisting of the aromatic rings.[27] The small, monovalent chloride ion clearly can accommodate this reorganization. However, in hybrids R_2ZnCl_4 and R_2CdCl_4, the metal halide anions are larger and divalent. Since the divalent metal halide anions are electrostatically interacting with two positively charged centers of the protonated stilbazole moieties, the lattice energy may increase and result in a higher barrier to renormalization, thus inhibiting dimerization.

In order to obtain further confirmation on the proposed organic derived emission mechanism, time-resolved PL was also done on both R_2ZnCl_4 and R_2CdCl_4 (Fig. 3). The decay profiles were fitting using the equation:

$$I(t) = I(t) = \int_0^t IRF(t') \left[I_0 + \sum_{i=1}^{n} A_i e^{-\frac{t-t'}{\tau_i}} \right] dt'$$

Here, $I(t)$ is the signal intensity, $IRF(t)$ is the prompt, I_0 is the dark counts (i.e. $\lim_{t\to\infty} I(t)$), n is the number of exponentials used, and τ is a lifetime. After refining, it was found that the average lifetime is 2.858 ns and 2.8630 ns for R_2ZnCl_4 and R_2CdCl_4, respectively. Using the following equation:

$$\frac{1}{\tau} = \frac{1}{\tau_0} + A_{nr}$$

one can calculate the radiative and non–radiative rates for both compounds. τ is the lifetime, τ_0 is the radiative lifetime, and A_{nr} represents the non-radiative rate. For R_2ZnCl_4, the radiative and non-radiative rates were calculated to be 3.63×10^7 s^{-1} and 3.13×10^8 s^{-1}, respectively. For R_2CdCl_4, radiative and non-radiative rates were calculated to be 3.92×10^7 s^{-1} and 3.49×10^8 s^{-1}, respectively. One characteristic of organic molecules is that they typically have faster emission lifetimes.[28] For both of our compounds, the emission lifetimes were on the single-digit nanosecond scale, supporting the attribution of PL emission to fast emission localized on the organic structural component.

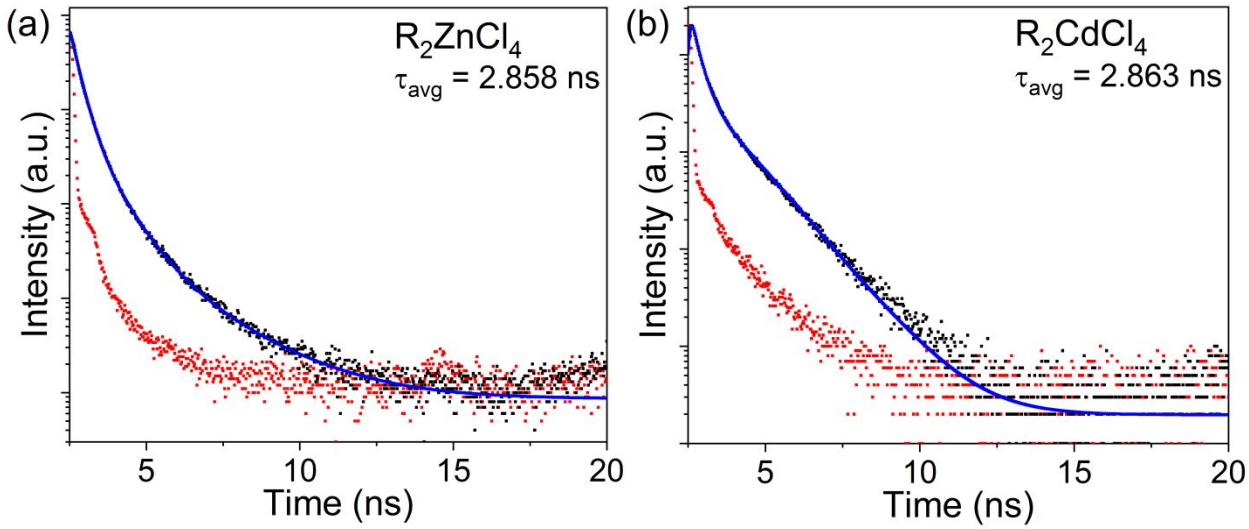

Fig. 3. Room temperature time-resolved PL for (a) R_2ZnCl_4 and (b) R_2CdCl_4 collected using an excitation wavelength of 442 nm.

Electronic structure calculations were performed for optimized structures of R_2MCl_4 (see Fig. S7). The band gaps for the optimized structures were calculated as 2.90 eV for R_2ZnCl_4 and 2.86 eV R_2CdCl_4 using the range separated hybrid functional HSE06, including spin-orbit coupling (SOC). These values are in a good agreement with the experimentally estimated band gaps obtained by transforming diffuse reflectance spectra via the Kubelka-Munk function. The estimated band gaps from the linear regions in the Kubelka-Munk plots are 2.78 eV for R_2ZnCl_4 and 2.65 eV for R_2CdCl_4 (Fig. S8). These band gap estimates are in close proximity to the PLE peaks at 2.79 eV and 2.74 eV for R_2ZnCl_4 and R_2CdCl_4, respectively. Note that when using the PBE exchange-correlation functional, the calculated band gaps are underestimated, as is expected due to the lack of exact exchange inclusion in the functional.

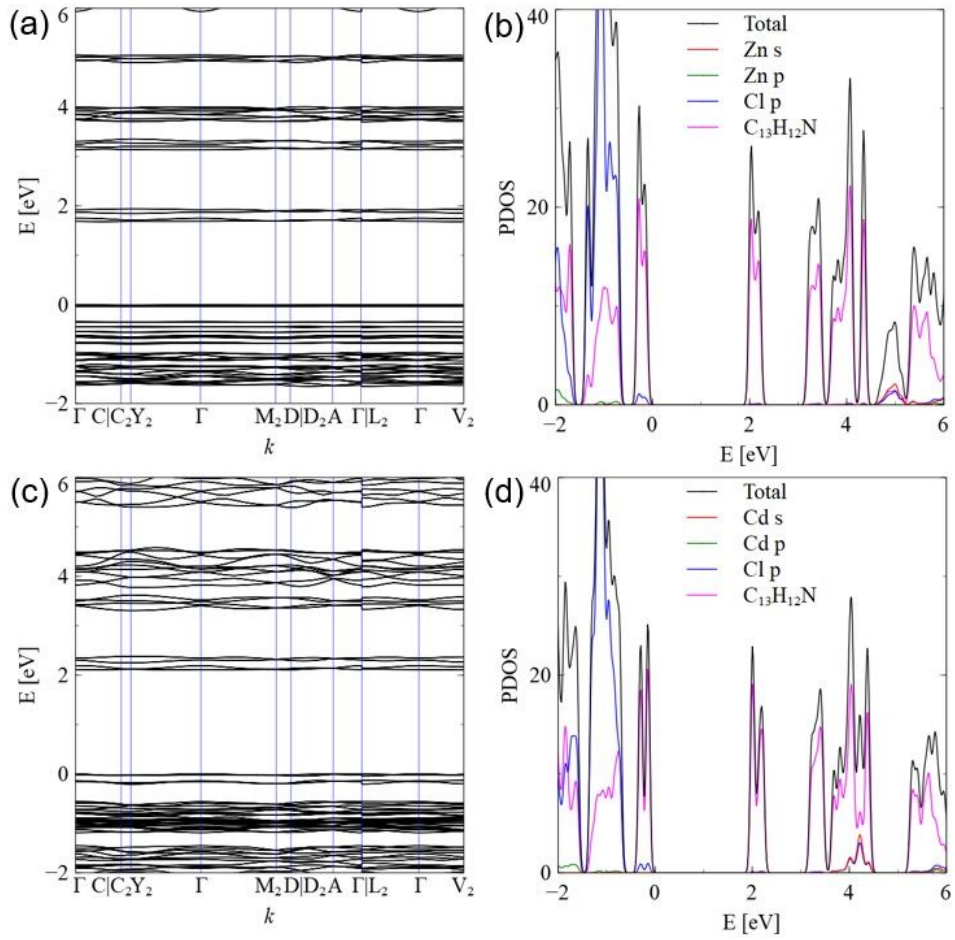

Fig. 4. Electronic band structures and density of states (DOS) plots for (a-b) R_2ZnCl_4 and (c-d) R_2CdCl_4.

The band structures and projected density of states (PDOS) are summarized in Fig. 4. As expected, band dispersions are overall weak because of van der Waals interactions. The PDOS for the inorganic components and organic cation (mauve color line) indicate that hybridization occurs near the valence band edge between the inorganic part and the organic cation, while the electronic states from the inorganic component are further away from the Fermi level for the conduction bands.

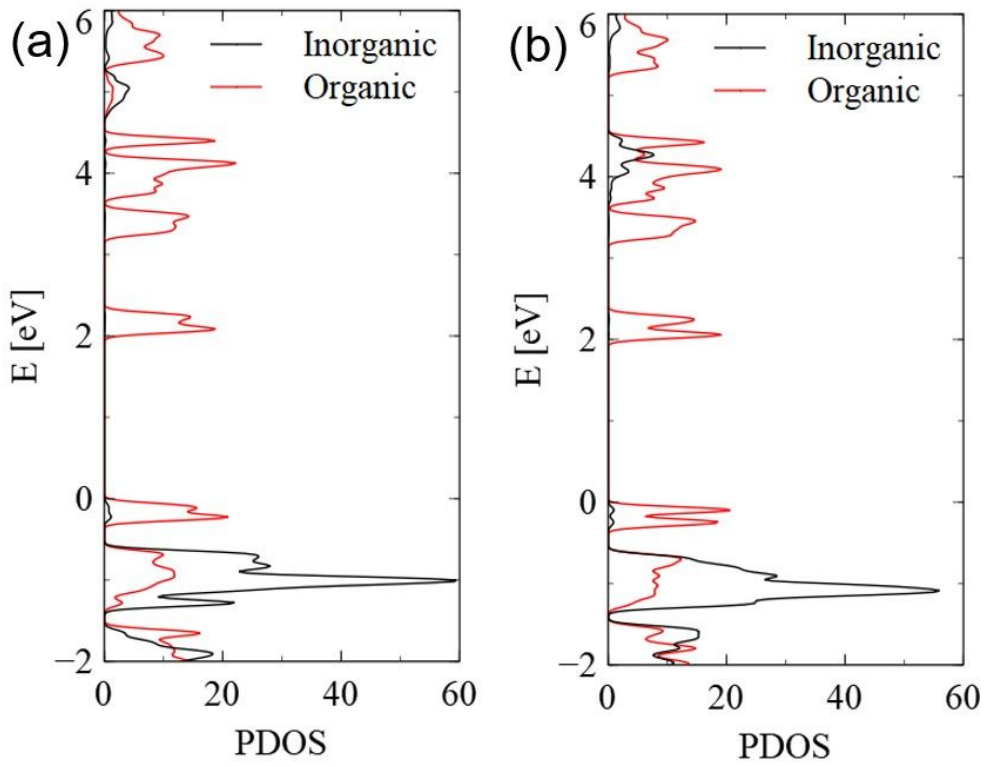

Fig. 5. PDOS for (a) R_2ZnCl_4 and (b) R_2CdCl_4 highlighting organic and inorganic contributions.

A detailed examination of the results (see Fig. 5) indicates that near the band gap the optical transitions primarily occur between the organic states near 2 eV in the conduction band, and organic states near 0 eV in the valence band; or between organic states near 2.0 eV in the conduction band, and a mixture of organic and inorganic states near -1.0 eV. Thus, below ca. 2.5 eV, the absorption is from the organic component, while above 2.5 eV, the absorption could involve organic and inorganic components. In addition, the increased PLQY for the hybrid materials is consistent with our suggestion of band hybridization. Importantly, DFT calculations support the attribution of PL emission to the organic molecular emission in R_2MCl_4.

Conclusion

In summary, we deliberately incorporated a light-emitting organic cation, (*E*)-4-styrylpyridinium (R^+), into a hybrid structure together with a large band gap metal halide to obtain R_2MCl_4 (M = Zn, Cd). The aim was to use the unconventional strategy of targeting a specific photoluminescent emission profile, by implementing a well-defined, photoactive organic cation as opposed to the traditional focus on metal halide photoluminescence. As intended, this selection of metal halide and organic components leads to an optical band gap dominated by the organic states in the valence and conduction band edges based on our DFT results. A thorough photoluminescence study on both the hybrid materials and organic salt, indicate a near identical emission profile throughout. Consequently, the observed green light emission in R_2MCl_4 is attributed to organic molecular emission.

We find that the incorporation of emissive organic molecules into hybrid structures has multiple key benefits. First, while the organic precursor itself is luminescent, the PL efficiency is enhanced nearly two-fold in the hybrid R_2MCl_4. Secondly, the organic salt has notably poor photostability due to photodimerization; RCl degrades rapidly, within 1 hour under continuous UV irradiation. The presence of tetrahedral metal chloride anions between the organic cations in R_2MCl_4 prevents the harmful photodimerization from occurring, which results in the dramatic improvement of their photostability. This work shows that design and optimization of hybrid organic-inorganic metal halide light emitters may not only target the inorganic structural component, but also organic molecular cation via the incorporation of photoemissive organic cations.

Acknowledgements

This material was based upon the work supported by the U.S. Department of Energy, Office of Science, Office of Basic Energy Sciences, under Award No. DE-SC0021158. We acknowledge Dr. Douglas R. Powell for the assistance with the single-crystal X-ray diffraction measurements (instrument support from NSF grant CHE-1726630).

Supporting Information

Single crystal X-ray diffraction data and refinement parameters, crystal images, PXRD, air and moisture stability test results, diffuse reflectance, TGA/DSC, CIE plots, and the DFT optimized cell.

Author Contributions

The manuscript was written through the contributions of all authors. All authors have approved the final version of the manuscript. T.C. and H.F., prepared the hybrid samples. I.G., B.E., and D.G. prepared the organic salt. T.C., H. F., and I.G. performed PXRD, TGA/DSC measurements, and analyzed the optical measurements. J.J. and R.P. carried out the theoretical calculations. B.S. conceived and supervised the work.

Author Information

Corresponding Author

Bayram Saparov - Department of Chemistry and Biochemistry, University of Oklahoma, 101 Stephenson Parkway, Norman, OK, USA; Email: saparov@ou.edu

Authors

Tielyr D. Creason – Department of Chemistry and Biochemistry, University of Oklahoma, 101 Stephenson Parkway, Norman, OK, USA

Hadiah Fattal – Department of Chemistry and Biochemistry, University of Oklahoma, 101 Stephenson Parkway, Norman, OK, USA

Isaiah W. Gilley – Department of Chemistry and Biochemistry, University of Oklahoma, 101 Stephenson Parkway, Norman, OK, USA

Brett N. Evans – Department of Chemistry and Biochemistry, University of Oklahoma, 101 Stephenson Parkway, Norman, OK, USA

Jie Jiang – Air Force Research Laboratory, Materials and Manufacturing Directorate, Wright-Patterson Air Force Base, OH, USA

Ruth Patcher – Air Force Research Laboratory, Materials and Manufacturing Directorate, Wright-Patterson Air Force Base, OH, USA

Daniel T. Glatzhofer – Department of Chemistry and Biochemistry, University of Oklahoma, 101 Stephenson Parkway, Norman, OK, USA

References

1. H. Lin, C. Zhou, Y. Tian, T. Siegrist and B. Ma, Low-Dimensional Organometal Halide Perovskites, *ACS Energy Lett.*, 2018, **3**, 54-62.
2. L. Protesescu, S. Yakunin, M. I. Bodnarchuk, F. Krieg, R. Caputo, C. H. Hendon, R. X. Yang, A. Walsh and M. V. Kovalenko, Nanocrystals of Cesium Lead Halide Perovskites ($CsPbX_3$, X = Cl, Br, and I): Novel Optoelectronic Materials Showing Bright Emission with Wide Color Gamut, *Nano Lett.*, 2015, **15**, 3692-3696.
3. M.-H. Du, Microscopic origin of multiple exciton emission in low-dimensional lead halide perovskites, *J. Chem. Phys.*, 2019, **151**, 181101.
4. M. Gao, C. Zhang, L. Lian, J. Guo, Y. Xia, F. Pan, X. Su, J. Zhang, H. Li and D. Zhang, Controlled synthesis and photostability of blue emitting $Cs_3Bi_2Br_9$ perovskite nanocrystals by employing weak polar solvents at room temperature, *J. Mater. Chem. C.*, 2019, **7**, 3688-3695.
5. T. D. Creason, T. M. McWhorter, Z. Bell, M.-H. Du and B. Saparov, K_2CuX_3 (X = Cl, Br): All-Inorganic Lead-Free Blue Emitters with Near-Unity Photoluminescence Quantum Yield, *Chem. Mat.*, 2020, **32**, 6197-6205.
6. W. Gao, L. Yin, J.-H. Yuan, K.-H. Xue, G. Niu, B. Yang, Q. Hu, X. Liu and J. Tang, Lead-free violet-emitting K_2CuCl_3 single crystal with high photoluminescence quantum yield, *Org. Electron.*, 2020, **86**, 105903.
7. R. Roccanova, A. Yangui, H. Nhalil, H. Shi, M.-H. Du and B. Saparov, Near-Unity Photoluminescence Quantum Yield in Blue-Emitting $Cs_3Cu_2Br_5$–xIx ($0 \leq x \leq 5$), *ACS Appl. Electron. Mater.*, 2019, **1**, 269–274.

8. Y. V. Morozov, S. Zhang, M. C. Brennan, B. Janko and M. Kuno, Photoluminescence Up-Conversion in $CsPbBr_3$ Nanocrystals, *ACS Energy Lett.*, 2017, **2**, 2514-2515.
9. T. D. Creason, A. Yangui, R. Roccanova, A. Strom, M.-H. Du and B. Saparov, Rb_2CuX_3 (X = Cl, Br): 1D All-Inorganic Copper Halides with Ultrabright Blue Emission and Up-Conversion Photoluminescence, *Adv. Opt. Mat.*, 2020, **8**, 1901338.
10. L. Dou, M. Lai, C. S. Kley, Y. Yang, C. G. Bischak, D. Zhang, S. W. Eaton, N. S. Ginsberg and P. Yang, Spatially resolved multicolor $CsPbX_3$ nanowire heterojunctions via anion exchange, *PNAS*, 2017, **114**, 201703860.
11. A. Yangui, S. Pillet, A. Mlayah, A. Lusson, G. Bouchez, S. Triki, Y. Abid and K. Boukheddaden, Structural phase transition causing anomalous photoluminescence behavior in perovskite $(C_6H_{11}NH_3)_2[PbI_4]$, *J. Chem. Phys.*, 2015, **143**, 224201.
12. S. Elleuch, T. Dammak, Y. Abid, A. Mlayah and H. Boughzala, Synthesis, structural and optical properties of a novel bilayered organic–inorganic perovskite $C_5Pb_2I_5$, *J. Lumin.*, 2010, **130**, 531-535.
13. V. Morad, Y. Shynkarenko, S. Yakunin, A. Brumberg, R. D. Schaller and M. V. Kovalenko, Disphenoidal Zero-Dimensional Lead, Tin, and Germanium Halides: Highly Emissive Singlet and Triplet Self-Trapped Excitons and X-ray Scintillation, *J. Am. Chem. Soc.*, 2019, **141**, 9764-9768.
14. K. M. McCall, V. Morad, B. M. Benin and M. V. Kovalenko, Efficient Lone-Pair-Driven Luminescence: Structure–Property Relationships in Emissive 5s2 Metal Halides, *ACS Mater. Lett.*, 2020, **2**, 1218-1232.
15. D. B. Straus, S. Hurtado Parra, N. Iotov, Q. Zhao, M. R. Gau, P. J. Carroll, J. M. Kikkawa and C. R. Kagan, Tailoring Hot Exciton Dynamics in 2D Hybrid Perovskites through Cation Modification, *ACS Nano*, 2020, **14**, 3621-3629.
16. T. D. Creason, H. Fattal, I. W. Gilley, T. M. McWhorter, M.-H. Du and B. Saparov, $(NH_4)_2AgX_3$ (X = Br, I): 1D Silver Halides with Broadband White Light Emission and Improved Stability, *ACS Mater. Au.*, 2021, **1**, 62-68.
17. A. Biswas, R. Bakthavatsalam, B. P. Mali, V. Bahadur, C. Biswas, S. S. K. Raavi, R. G. Gonnade and J. Kundu, The metal halide structure and the extent of distortion control the photo-physical properties of luminescent zero dimensional organic-antimony(iii) halide hybrids, *J. Mater. Chem. C.*, 2021, **9**, 348-358.
18. Y. Wei, Z. Cheng and J. Lin, An overview on enhancing the stability of lead halide perovskite quantum dots and their applications in phosphor-converted LEDs, *Chem. Soc. Rev.*, 2019, **48**, 310-350.
19. M. Wu, N. Haji Ladi, Z. Yi, H. Li, Y. Shen and M. Wang, Stability Issue of Perovskite Solar Cells under Real-World Operating Conditions, *Energy Technol. (Weinheim, Ger.)*, 2020, **8**, 1900744.
20. S. Lu, Q. Zhou, Y. Ouyang, Y. Guo, Q. Li and J. Wang, Accelerated discovery of stable lead-free hybrid organic-inorganic perovskites via machine learning, *Nature Communications*, 2018, **9**, 3405.
21. Y. Li and K. Yang, High-throughput computational design of organic–inorganic hybrid halide semiconductors beyond perovskites for optoelectronics, *Energy & Environmental Science*, 2019, **12**, 2233-2243.
22. X. Mo, T. Li, F. Huang, Z. Li, Y. Zhou, T. Lin, Y. Ouyang, X. Tao and C. Pan, Highly-efficient all-inorganic lead-free 1D $CsCu_2I_3$ single crystal for white-light emitting diodes and UV photodetection, *Nano Energy*, 2020, **81**, 105570.

23. Y.-C. Lin, M. Karlsson and M. Bettinelli, Inorganic Phosphor Materials for Lighting, *Top. Curr. Chem.*, 2016, **374**, 21.
24. A. Yangui, R. Roccanova, T. M. McWhorter, Y. Wu, M.-H. Du and B. Saparov, Hybrid Organic–Inorganic Halides $(C_5H_7N_2)_2MBr_4$ (M = Hg, Zn) with High Color Rendering Index and High-Efficiency White-Light Emission, *Chem. Mater.*, 2019, **31**, 2983-2991.
25. A. Yangui, R. Roccanova, Y. Wu, M.-H. Du and B. Saparov, Highly Efficient Broad-Band Luminescence Involving Organic and Inorganic Molecules in a Zero-Dimensional Hybrid Lead Chloride, *The Journal of Physical Chemistry C*, 2019, **123**, 22470-22477.
26. G. M. J. Schmidt, Photodimerization in the solid state, *Pure Appl. Chem.*, 1971, **27**, 647-678.
27. S. Yamada, N. Uematsu and K. Yamashita, Role of Cation−π Interactions in the Photodimerization of trans-4-Styrylpyridines, *J. Am. Chem. Soc.*, 2007, **129**, 12100-12101.
28. H. Fattal, T. D. Creason, C. J. Delzer, A. Yangui, J. P. Hayward, B. J. Ross, M.-H. Du, D. T. Glatzhofer and B. Saparov, Zero-Dimensional Hybrid Organic–Inorganic Indium Bromide with Blue Emission, *Inorg. Chem.*, 2021, **60**, 1045-1054.
29. R. Roccanova, M. Houck, A. Yangui, D. Han, H. Shi, Y. Wu, D. T. Glatzhofer, D. R. Powell, S. Chen, H. Fourati, A. Lusson, K. Boukheddaden, M.-H. Du and B. Saparov, Broadband Emission in Hybrid Organic–Inorganic Halides of Group 12 Metals, *ACS Omega*, 2018, **3**, 18791-18802.
30. R. Roccanova, W. Ming, V. R. Whiteside, M. A. McGuire, I. R. Sellers, M. H. Du and B. Saparov, Synthesis, Crystal and Electronic Structures, and Optical Properties of $(CH_3NH_3)_2CdX_4$ (X = Cl, Br, I), *Inorg. Chem.*, 2017, **56**, 13878-13888.
31. F. Tessore, G. Di Carlo, A. Forni, S. Righetto, F. Limosani and A. Orbelli Biroli, Second Order Nonlinear Optical Properties of 4-Styrylpyridines Axially Coordinated to A4 ZnII Porphyrins: A Comparative Experimental and Theoretical Investigation, *Inorganics*, 2020, **8**.
32. J. Pang, Z. Deng, S. Sun, G. Huang, G. Zhang, A. Islam, L. Dang, D. L. Phillips and M.-D. Li, Unprecedentedly Ultrafast Dynamics of Excited States of C═C Photoswitching Molecules in Nanocrystals and Microcrystals, *J. Phys. Chem. Lett.*, 2021, **12**, 41-48.
33. H. Goerner, Phosphorescence of trans-stilbene, stilbene derivatives, and stilbene-like molecules at 77 K, *J. Phys. Chem.*, 1989, **93**, 1826-1832.
34. U. Mazzucato, G. G. Aloisi and F. Masetti, Role of charge transfer interactions in photoreactions III: inorganic anion-induced intersystem crossing of stilbene-like molecules, *J. Photochem.*, 1982, **18**, 211-222.
35. A. Briceño and Y. Hill, Exploring the use of anionic homoleptic complexes as templates in the design of photoreactive multi-component supramolecular assemblies, *CrystEngComm*, 2012, **14**, 6121-6125.
36. J. R. Nickell, J. P. Culver, V. Janganati, G. Zheng, L. P. Dwoskin and P. A. Crooks, 1,4-Diphenalkylpiperidines: A new scaffold for the design of potent inhibitors of the vesicular monoamine transporter-2, *Bioorg Med Chem Lett*, 2016, **26**, 2997-3000.
37. T. B. Nguyen, T. M. Nguyen and P. Retailleau, [2+2] Photodimerization of Stilbazoles Promoted by Oxalic Acid in Suspension, *Chemistry – A European Journal*, 2020, **26**, 4682-4689.
38. J. M. Smith, H. W. Stewart, B. Roth and E. H. Northey, α-Aminophenacylpyridines and Quinolines1, *J. Am. Chem. Soc.*, 1948, **70**, 3997-4000.

39. S. Yamada and Y. Nojiri, Water-assisted assembly of (E)-arylvinylpyridine hydrochlorides: effective substrates for solid-state [2+2] photodimerization, *Chemical Communications*, 2011, **47**, 9143-9145.
40. G. Kresse and J. Furthmüller, Efficiency of ab-initio total energy calculations for metals and semiconductors using a plane-wave basis set, *Computational Materials Science*, 1996, **6**, 15-50.
41. G. Kresse and D. Joubert, From ultrasoft pseudopotentials to the projector augmented-wave method, *Physical Review B*, 1999, **59**, 1758-1775.
42. J. P. Perdew, K. Burke and M. Ernzerhof, Generalized Gradient Approximation Made Simple, *Physical Review Letters*, 1996, **77**, 3865-3868.
43. S. Grimme, J. Antony, S. Ehrlich and H. Krieg, A consistent and accurate ab initio parametrization of density functional dispersion correction (DFT-D) for the 94 elements H-Pu, *J. Chem. Phys.*, 2010, **132**, 154104.
44. H. Beck, C. Gehrmann and D. A. Egger, Structure and binding in halide perovskites: Analysis of static and dynamic effects from dispersion-corrected density functional theory, *APL Materials*, 2019, **7**, 021108.
45. L. Zhang and W. Liang, How the structures and properties of two-dimensional layered perovskites MAPbI3 and CsPbI3 vary with the number of layers, *The journal of physical chemistry letters*, 2017, **8**, 1517-1523.
46. R. Shannon, Revised effective ionic radii and systematic studies of interatomic distances in halides and chalcogenides, *Acta Crystallogr. A.*, 1976, **32**, 751-767.
47. X. Zhang, L. Li, S. Wang, X. Liu, Y. Yao, Y. Peng, M. Hong and J. Luo, [(N-AEPz)$ZnCl_4$]Cl: A "Green" Metal Halide Showing Highly Efficient Bluish-White-Light Emission, *Inorg. Chem.*, 2020, **59**, 3527-3531.
48. T. M. McWhorter, Z. Zhang, T. D. Creason, L. Thomas, M.-H. Du and B. Saparov, $(C_7H_{11}N_2)_2MBr_4$ (M=Cu, Zn): X-Ray Sensitive 0D Hybrid Metal Halides with Tunable Broadband Emission, *Eur. J. Inorg. Chem.*, 2022, **n/a**, e202100954.
49. M. V. Veidis, G. H. Schreiber, T. E. Gough and G. J. Palenik, Jahn-Teller distortions in octahedral copper(II) complexes, *J. Am. Chem. Soc.*, 1969, **91**, 1859-1860.
50. W. J. Crama and W. J. A. Maaskant, On the cooperative Jahn-Teller effect in ternary chromium and copper halides, *Physica B+C*, 1983, **121**, 219-232.
51. C. Sun, W.-L. He, M.-J. Liu, W.-J. Pan, L.-F. Dong, G. Chen, G.-D. Liu and X.-W. Lei, Zero-Dimensional Hybrid Cd-Based Perovskites with Broadband Bluish White-Light Emissions, *Chem. - Asian J.*, 2020, **15**, 3050-3058.
52. O. Y. Vassilyeva, E. A. Buvaylo, Y. V. Lobko, R. P. Linnik, V. N. Kokozay and B. W. Skelton, Organic–inorganic hybrid tetrachlorocadmates as promising fluorescent agents for cross-linked polyurethanes: synthesis, crystal structures and extended performance analysis, *RSC Advances*, 2021, **11**, 7713-7722.
53. W.-Q. Liao, H.-Y. Ye, D.-W. Fu, P.-F. Li, L.-Z. Chen and Y. Zhang, Temperature-Triggered Reversible Dielectric and Nonlinear Optical Switch Based on the One-Dimensional Organic-Inorganic Hybrid Phase Transition Compound [C6H11NH3]2CdCl4, *Inorg. Chem.*, 2014, **53**, 11146-11151.
54. X.-F. Sun, Z. Wang, P.-F. Li, W.-Q. Liao, H.-Y. Ye and Y. Zhang, Tunable Dielectric Responses Triggered by Dimensionality Modification in Organic-Inorganic Hybrid Phase Transition Compounds (C5H6N)CdnCl2n+1 (n = 1 and 2), *Inorg. Chem.*, 2017, **56**, 3506-3511.

55. C. Sun, Q.-Q. Zhong, X. Zhang, P.-C. Xiao, Y. Cheng, Y.-J. Gao, G.-D. Liu and X.-W. Lei, A Zero-Dimensional Hybrid Cadmium Perovskite with Highly Efficient Orange-Red Light Emission, *Inorg. Chem.*, 2021, **60**, 18879-18888.
56. O. Y. Vassilyeva, E. A. Buvaylo, V. N. Kokozay, B. W. Skelton and A. N. Sobolev, Crystal structures of an imidazo[1,5-a]pyridinium-based ligand and its $(C_{13}H_{12}N_3)_2[CdI_4]$ hybrid salt, *Acta Crystallogr. E.*, 2019, **75**, 1209-1214.
57. M. Horner and S. Huenig, Bicyclo[1.1.0]butanes. A new synthetic route and valence isomerizations, *J. Am. Chem. Soc.*, 1977, **99**, 6120-6122.